Aging Cell (2013) **12**, pp93–101 Doi: 10.1111/acel.12025

A metabolic signature predicts biological age in mice

Antonia Tomás-Loba,[1#] Bruno Bernardes de Jesus,[1#] Jose M. Mato[2] and Maria A. Blasco[1]

[1]Telomeres and Telomerase Group, Molecular Oncology Program, Spanish National Cancer Research Centre (CNIO), Melchor Fernández Almagro 3, Madrid, E-28029, Spain
[2]CIC bioGUNE, CIBERehd, Derio, Technology Park of Bizkaia, Derio, E-48160, Spain

Summary

Our understanding of the mechanisms by which aging is produced is still very limited. Here, we have determined the sera metabolite profile of 117 wild-type mice of different genetic backgrounds ranging from 8 to 129 weeks of age. This has allowed us to define a robust metabolomic signature and a derived metabolomic score that reliably/accurately predicts the age of wild-type mice. In the case of telomerase-deficient mice, which have a shortened lifespan, their metabolomic score predicts older ages than expected. Conversely, in the case of mice that overexpress telomerase, their metabolic score corresponded to younger ages than expected. Importantly, telomerase reactivation late in life by using a TERT-based gene therapy recently described by us significantly reverted the metabolic profile of old mice to that of younger mice, further confirming an anti-aging role for telomerase. Thus, the metabolomic signature associated with natural mouse aging accurately predicts aging produced by telomere shortening, suggesting that natural mouse aging is in part produced by presence of short telomeres. These results indicate that the metabolomic signature is associated with the biological age rather than with the chronological age. This constitutes one of the first aging-associated metabolomic signatures in a mammalian organism.

Key words: aging; life-span studies; mouse; mTERT; Telomerase; Telomere.

High-throughput metabolite profiling technologies can be used to determine the metabolic status of whole organisms under conditions of interest, as well as to systematically define phenotypic patterns associated with mutant genotypes (Raamsdonk *et al.*, 2001; Allen *et al.*, 2003; Nicholson & Wilson, 2003; Lewis *et al.*, 2010). Here, we set to determine the metabolic profile of wild-type mice at different ages with the goal of obtaining a metabolomic signature of natural mouse aging, which could serve as a predictive model to estimate the biological age, as well as that could allow to identify new biomarkers of aging. Furthermore, we reasoned that analysis of this age-related metabolomic signature in short-lived, telomerase-deficient (*Terc*$^{-/-}$), and long-lived TERT transgenics mice could serve to assess the contribution of telomere shortening and telomerase status to the metabolomic changes associated with natural mouse aging (Blasco *et al.*, 1997; Lee *et al.*, 1998; Herrera *et al.*, 1999; Garcia-Cao *et al.*, 2006; Tomas-Loba *et al.*, 2008). A liquid chromatography–mass spectrometry (UPLC-MS) platform–based metabolomics approach was used to explore the relative levels of serum metabolites during mouse aging. To circumvent the potential influence of genetic background and gender in the metabolomic profile associated with mouse aging, 117 serum samples were analyzed from wild-type mice of different genetic backgrounds (see Materials and methods), and these samples included sera from both male (51) and female (66) mice with ages ranging from 8 to 129 weeks. Furthermore, we also determined the metabolomic profiles of middle-aged (1 year) and old (2 years) control wild-type mice compared with that of 2-year-old mice treated with a TERT-based gene therapy recently shown by us to reactivate telomerase and delay aging (see Materials and methods) (Bernardes de Jesus *et al.*, 2012). The only phenotypic distinction we have analyzed in this manuscript is age. This could be viewed as one limitation of this study as co-founding effects (such as disease or obesity) were not taken into account.

The global metabolite profile was processed to create a multivariate model correlating the spectral data with the age of the wild-type samples. A predictive PLS model (Projection to Latent Structure; see Materials and methods) was built and validated (Figure S1), obtaining a robust metabolomic model of aging for wild-type mice, which fits well a linear model (r^2 = 0.944) (closed black diamonds in Fig. 1A). Variable influence on projection (VIP) parameters and Spearman's rank correlation coefficients (ρ) were examined for each metabolite, identifying the most influential biomarkers in the PLS model and aging – correlative. Table 1 highlights selection of 48 biomarkers for which there is a significant correlation of wild-type samples with age (Spearman's rank correlation test *P*-values < 0.05). These biomarkers include phospholipids, fatty acids, and organic acids, in agreement with the fact that the extraction methodology provides a maximum coverage over those families of compounds.

We then used this wild-type mouse metabolomic signature of aging to predict the ages of first-generation (G1) mice deficient in telomerase activity due to deletion of the telomerase RNA component or *Terc* (G1 *Terc*$^{-/-}$ mice). These mice show premature aging and decreased median and maximum longevity already at the first generation (Blasco *et al.*, 1997; Lee *et al.*, 1998; Herrera *et al.*, 1999; Garcia-Cao *et al.*, 2006). Interestingly, G1 *Terc*$^{-/-}$ mice showed a significantly older (*P*-value = 1.011 e^{-8}) metabolic age when compared with wild-type mice of the same chronological age (red circles in Fig. 1A). Thus, the metabolomic signature associated with physiological wild-type mouse aging accurately predicts aging produced by short telomeres owing to telomerase deficiency. These results suggest that physiological mouse aging is largely associated with the presence of short telomeres or to cellular conditions favoring telomere protection, such an increased load of tumor suppressors (Tomas-Loba *et al.*, 2008). Indeed, the increase in the rate of increase of short telomeres was recently shown to be correlated with the realized lifespan in mice (Vera *et al.*, 2012). Next, we used our wild-type mouse aging metabolomic signature to predict the ages of transgenic mice overexpressing the telomerase reverse-transcriptase subunit or TERT in various stratified epithelia (*K5-TERT mice*). We have previously shown that *K5-TERT* mice have increased tissue fitness and a delayed aging (Gonzalez-Suarez *et al.*, 2001, 2005). Serum metabolomic profiles were not significantly different when comparing

Correspondence
Maria A. Blasco, Spanish National Cancer Research Centre (CNIO), 3 Melchor Fernandez Almagro street, Madrid E-28029, Spain. Tel.: +34.91.732.8031; fax: +34.91.732.8028; e-mail: mblasco@cnio.es

[#]These authors equally contributed to this work.

Accepted for publication *19 October 2012*

Aging Cell

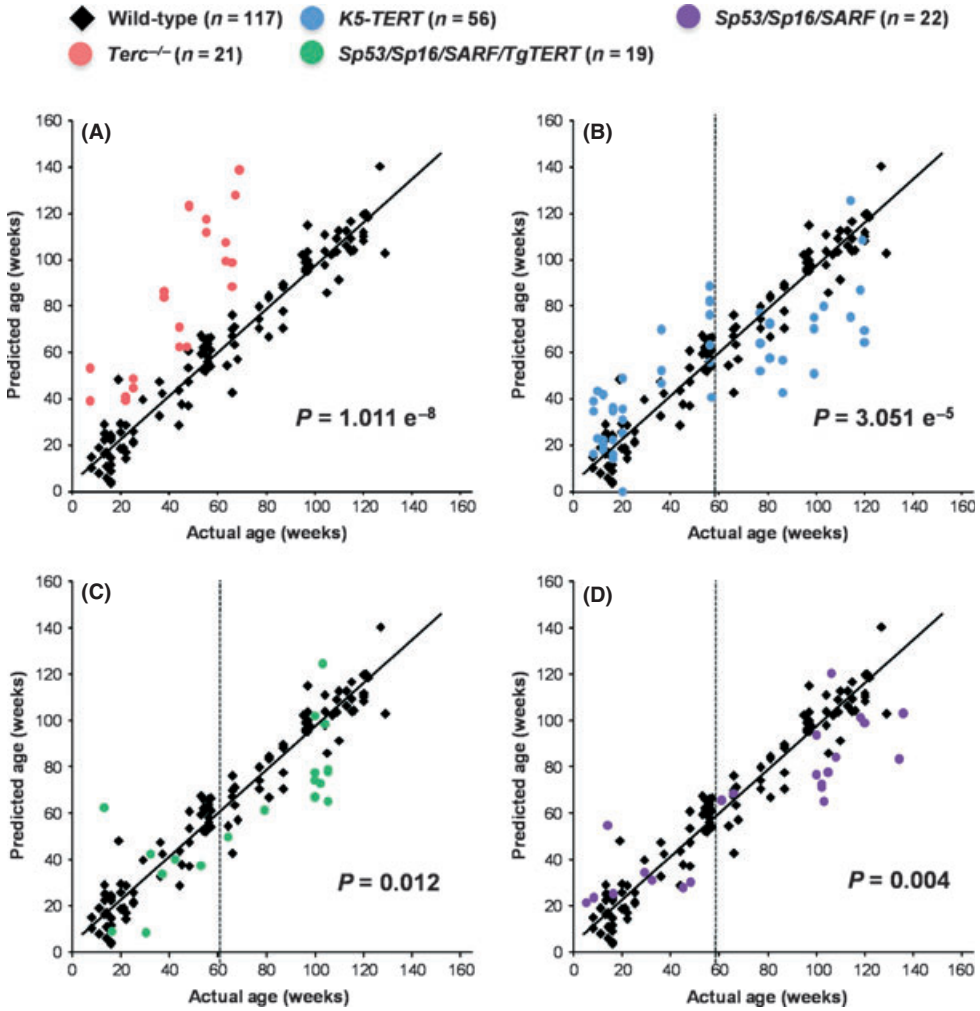

Fig. 1 Age predictions with respect to the wild-type mice metabolomic signature. The wild-type mice metabolomic aging changes (black diamonds) fit a linear model: predicted age = 0.934·Actual Age + 3.971 (r^2 = 0.944). (A) G1 *Terc*$^{-/-}$ samples (red circles); (B) *K5-Tert* samples (blue circles); (C) *Sp53/Sp16/Sp19Arf/K5-Tert* samples (green circles); (D) *Sp53/Sp16/Sp19Arf* samples (purple circles). *P*-values for Figure B–D correspond only to mice over 60 months of age.

wild-type and TERT overexpressing mice of all age groups (5–140 weeks; *P*-value = 0.534) (blue circles, Fig. 1B). However, when we compared metabolic profiles of only adult/old mice (ages ranging from 60–140 weeks old), mice overexpressing TERT showed a significantly younger (*P*-value = 3.051 e^{-5}) metabolic age than wild-type animals (Fig. 1B). To circumvent the cancer-promoting activity of telomerase, we also determined the metabolomic profile of our recently generated TERT overexpressing mice with enhanced cancer resistance owing to increased expression of the tumor suppressors p53, p16, and p19ARF (Sp53/Sp16/SARF/TgTERT). Sp53/Sp16/SARF/TgTERT mice show a delayed aging and a 40% extension of the median lifespan (Tomas-Loba *et al.*, 2008). Serum metabolomic profiles of Sp53/Sp16/SARF/TgTERT mice identified significant differences in metabolic age compared with wild-type mice of the same chronological age, although the differences were not very robust (*P*-value = 0.031) when the complete range of ages (8–140 weeks old) was evaluated (green circles in Fig. 1C). Again, when we compared the metabolic profile of adult/old Sp53/Sp16/SARF/TgTERT mice ranging in age from 60 to 140 weeks old, Sp53/Sp16/SARF/TgTERT mice showed a significantly younger (*P*-value = 0.012) metabolic age compared with wild-type mice of the same chronological age (green circles in Fig. 1C). Delayed organismal aging and extended lifespan have also been demonstrated through improved damage protection by increasing the activity of the p53/ARF pathway in Sp53/Sp16/SARF mice (Matheu *et al.*, 2007). Comparison of serum metabolomic profiles from Sp53/Sp16/SARF and wild-type mice identified modest but significant differences (*P*-value = 0.045) when the complete range of ages (8–140 weeks old) was evaluated (purple circles, Fig. 1D). These differences became more significant (*P*-value = 0.004) when only adult/old mice (ages ranging between 60 and 140 weeks old) were compared (purple circles, Fig. 1D), indicating that old Sp53/Sp16/SARF mice have significantly younger metabolic ages than age-matched wild-type mice. Together, these results support an impact of telomerase activity and telomere length, as well as of the p53/p16/p19ARF tumor suppressors, on the metabolomic profile associated with natural mouse aging.

Next, we followed the behavior of different metabolites associated wth mouse aging. Figure 2 shows representative examples of selected biomarkers in sera from wild-type, G1 *Terc*$^{-/-}$, and TERT transgenic mice at various ages. Figure 2A,C,D, corresponding to a not determined metabolite (*Rt* = 7.4 min; *m/z* = 776.5798), sphingomyelin SM(d18:1/16:1), and glycerophosphoethanolamine PE(P-16:0/22:6), respectively,

Table 1 Selection of aging serum metabolic biomarkers

Rt (min)	*m/z* (Da/e)	Ion	ID	Spearman's rho	*P*-value	VIP
7.11	774.5646	$[M+H]^+$	ND	−0.64987	5.23×10^{-11}	3.335
6.90	719.5687	$[M+H]^+$	ND	−0.54365	1.56×10^{-7}	2.999
3.67	378.2400	$[M-H]^-$	Sphingosine 1 – phosphate	−0.50817	1.28×10^{-6}	0.917
6.52	608.4578	ND	ND	−0.49980	2.03×10^{-6}	1.264
6.54	717.5526	ND	ND	−0.47733	6.62×10^{-6}	2.166
6.78	745.5492	$[M+FA]^-$	SM(d18:1/16:1)	−0.46557	1.19×10^{-5}	1.492
7.40	776.5789	$[M+H]^+$	ND	−0.39461	2.67×10^{-4}	3.393
4.74	480.3082	$[M-H]^-$	LysoPE(18:0)	−0.38019	4.64×10^{-4}	0.944
3.81	542.3239	$[M+H]^+$	LysoPC(20:5)	0.37572	5.47×10^{-4}	1.460
0.62	160.1316	$[M+H]^+$	2-aminooctanoic acid	0.36586	7.83×10^{-4}	1.896
0.82	204.1236	$[M+H]^+$	L-Acetylcarnitine	−0.32805	2.79×10^{-3}	1.161
0.60	147.0769	$[M+H]^+$	Glutamine	−0.31736	3.89×10^{-3}	1.445
7.50	826.5595	$[M+FA]^-$	PC(18:2/18:2)	−0.31388	4.32×10^{-3}	0.929
2.98	481.2043	ND	ND	−0.31254	4.50×10^{-3}	1.044
4.25	502.2935	$[M+FA-MFA]^-$	LysoPE(20:3)	−0.29817	6.86×10^{-3}	1.738
6.02	305.2474	$[M-H]^-$	Eicosatrienoic acid	0.29803	6.89×10^{-3}	0.916
7.88	722.5129	$[M-H]^-$	PE(P-16:0/20:4)	−0.29592	7.31×10^{-3}	1.221
7.31	774.5367	$[M+FA]^-$	PE(14:0/18:2)	−0.29171	8.23×10^{-3}	1.528
0.84	150.0588	$[M+H]^+$	L-Methionine	−0.28323	0.0104	0.857
5.38	269.2268	ND	ND	0.28115	0.0110	1.054
7.17	747.5637	$[M+FA]^-$	SM(d18:1/16:0)	−0.27966	0.0115	1.060
4.17	452.2764	$[M-H]^-$	LysoPE(16:0)	−0.27951	0.0115	1.134
6.76	721.5845	$[M+H]^+$	ND	−0.27871	0.0118	0.877
7.70	768.5907	$[M+H]^+$	ND	−0.27472	0.0131	0.970
6.61	447.3831	ND	ND	−0.26165	0.0183	1.231
7.29	773.5794	$[M+FA]^-$	SM(36:2)	−0.25655	0.0208	1.373
0.60	132.0771	$[M+H]^+$	Creatine	−0.25449	0.0219	1.383
7.91	778.5623	$[M+FA]^-$	PC(16:0/16:0)	−0.24690	0.0263	1.108
7.74	772.5875	$[M+H]^+$	PC(17:0/18:2)	−0.24509	0.0274	1.162
6.97	778.5341	ND	ND	0.24449	0.0278	1.136
0.61	116.0710	$[M+H]^+$	Proline	−0.24321	0.0287	1.263
4.63	536.3651	ND	ND	0.24095	0.0302	1.096
7.38	744.5543	$[M+H]^+$	PC(15:0/18:2)	−0.24050	0.0306	1.347
7.60	716.5233	$[M+H]^+$	PE(16:0/18:2)	−0.23397	0.0355	1.164
7.60	748.5272	$[M+H]^+$	PE(P-16:0/22:6)	−0.22895	0.0398	1.203
0.55	167.0198	$[M-H]^-$	Uric acid	0.22832	0.0404	1.605
7.46	764.5225	$[M+H]^+$	PE(16:0/22:6)	−0.22750	0.0411	1.109
5.84	325.3203	ND	ND	0.22342	0.0450	1.125
7.42	800.5449	$[M+FA]^-$	PC(34:3)	−0.22217	0.0462	0.964
5.39	296.2590	$[M+ACN+H]^+$	Palmitoleic acid	0.21926	0.0492	0.944
0.57	124.0079	$[M+H]^+$	Taurine	0.25912	0.0195	0.718
4.22	279.2307	$[M+H]^+$	Linolenic acid	0.27863	0.0118	0.717
5.99	283.2627	$[M+H]^+$	Oleic acid	0.24274	0.0290	0.739
6.61	652.4550	ND	ND	−0.33682	2.11×10^{-3}	0.797
7.47	850.5606	$[M+H]^+$	PC(16:0/22:6)	−0.24003	0.0309	1.090
7.50	832.5889	$[M+H]^+$	PC(40:7)	0.27525	0.0129	0.604
7.99	808.5871	$[M+H]^+$	PC(38:5)	0.27729	0.0122	0.860
8.11	766.5396	$[M+H]^+$	PE(38:4)	−0.38345	4.10×10^{-4}	1.135

Peaks are listed for which there is significant correlation of wild-type samples with age [Spearman's rank correlation test *P*-values < 0.05]. *Rt* (min), chromatographic retention time; *m/z* (Da/e) [*m* is the neutral molecular mass value, *e* is the elemental charge], mass-to-charge ratio of ion detected; Ion, most intense species observed; ID, metabolite name (lipid names follow the LIPID MAPS classification system for lipids www.lipidmaps.org); Spearman's rho, Spearman's rank correlation coefficient; *P*-value, *P*-value derived from the Spearman's rank correlation coefficient; VIP, variable influence on projection parameter. ND, not determined.

exemplify the metabolic discrimination of G1 $Terc^{-/-}$ mice from the other sample groups. In particular, the relative decrease in abundance of these biomarkers occurs on a much faster timescale for the G1 $Terc^{-/-}$ mutants than for wild-type mice or TERT transgenics. Figure 2B illus trates a biomarker, lysoglicerophosphocholine [LysoPC(18:3)], showing distinct temporal evolutions in the 3 sample groups. In particular, its relative intensity remains more or less constant over time for the TERT transgenics, while a marked decrease with age is observed for wild-type and G1 $Terc^{-/-}$ mice, the relative change once more occurring much quicker in the latter group. Opposite trends (increased rather than decreased relative intensities) are shown in Fig. 2E,F, corresponding to glycerophosphoethanolamines PE(16:0/18:2) and PE(16:0/22:6), respec-

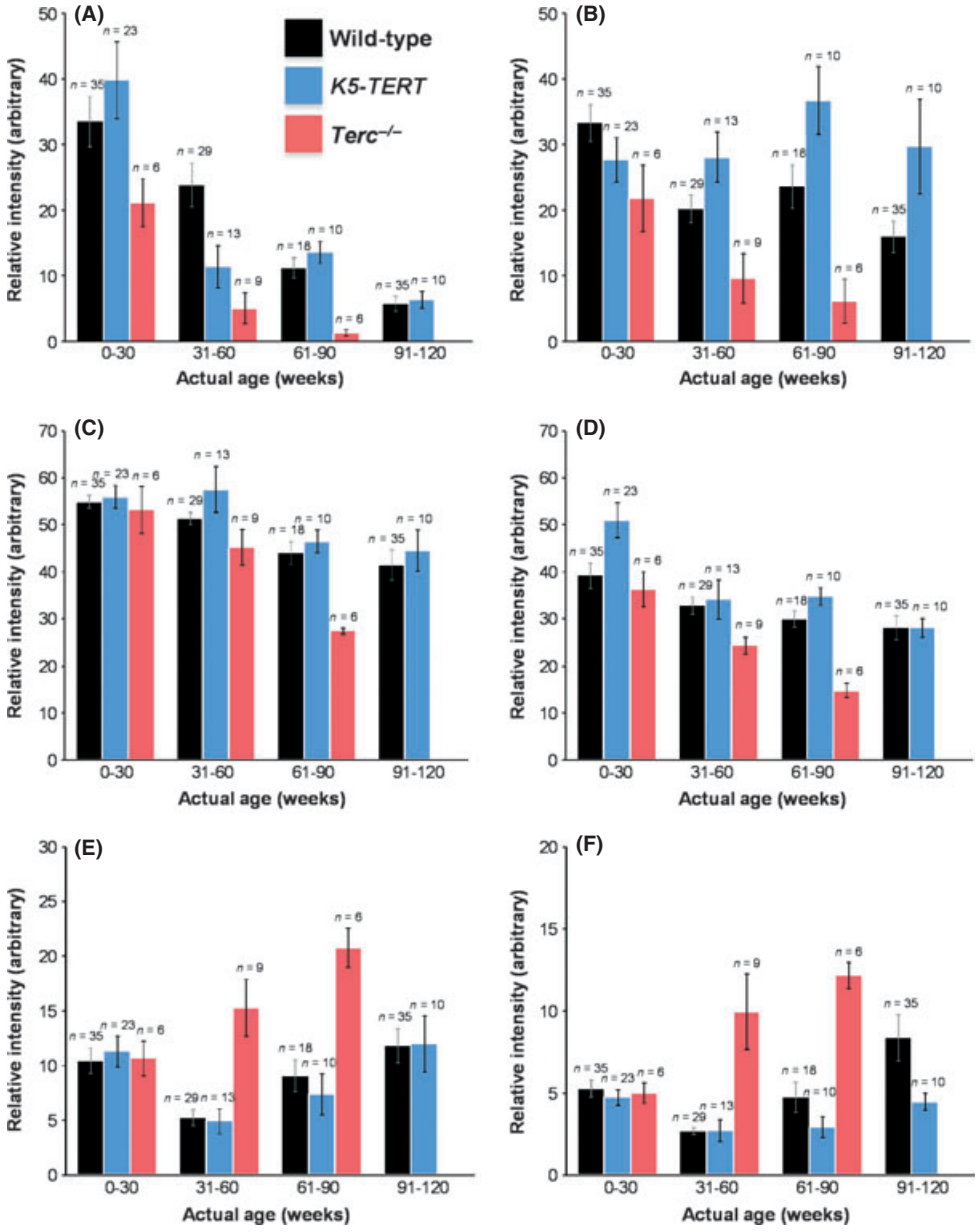

Fig. 2 Metabolite profile plots (mean ± 1 standard error of the mean). (A) *Rt* = 7.4 min, *m/z* = 776.5789 (not determined); (B) LysoPE(20:3); (C) SM(d18:1/16:1); (D) PE(P-16:0/22:6); (E) PE(16:0/18:2); (F) PE(16:0/22:6). WT samples (black); *K5-Tert* samples (blue); *Terc*$^{-/-}$ samples (red).

tively. Both of these biomarkers increase rapidly with age in the *Terc*$^{-/-}$ cohorts, while a less pronounced change is observed in WT mice. The intensities of these biomarkers do not show significant changes over time in the TERT transgenic group. Interestingly, some of the metabolites identified here (i.e., sphingomyelin, glycerophosphoethanolamines) have been previously linked to neurodegenerative disorders and various aspects of aging and disease (Klunk *et al.*, 1997; Cutler & Mattson, 2001).

Recently, we reported that telomerase expression late in life by using a TERT-based gene therapy strategy was sufficient to delay age-associated decay and to significantly extend mouse longevity (Bernardes de Jesus *et al.*, 2012). Among other beneficial effects of TERT treatment, we observed that mice treated with AAV9-TERT showed improved metabolic parameters including a better performance in glucose and insulin tolerance tests. To dissect the effects of TERT treatment on metabolism, here, we studied the metabolomics profiles of 1- and 2-year-old mice treated with TERT (AAV9-mTERT) or with a control vector (AAV9-eGFP). To this end, we first compared the metabolomics profile of 1-year-old and 2-year-old control mice treated with AAV9-eGFP, which allowed to establish a set of metabolites that changed associated with aging (Table 2). Interestingly, we found that 2 months after TERT treatment, old mice (2 years old) showed a reversal of the metabolic signature associated with aging (Fig. 3). In particular, 2-year-old mice treated with AAV9-mTERT showed a metabolic signature, which resembled the signature presented by the 1-year-old control mice. Therefore, expression of telomerase in aged mice partially rescues the

Table 2 Selection of biomarkers distinguishing 1- and 2-year old AAV9-GFP and comparison of 2-year-old AAV9-GFP- and AAV9-TERT-treated mice

				AAV9-eGFP 2-year-old/1-year-old		2-year-old AAV9-mTERT/2-year-old AAV9-eGFP	
Rt (min)	*m/z* (Da/e)	Ion	ID	Fold change	*P*-value	Fold change	*P*-value
6.15	717.5180	$[M+FA]^-$	SM32:2	0.36	1.12×10^{-6}	2.63	1.30×10^{-6}
3.88	564.3295	$[M+FA]^-$	LysoPC(18:2)	0.60	1.62×10^{-6}	1.52	1.34×10^{-4}
6.42	283.2631	$[M-H]^-$	(18/0) Stearic acid	0.48	1.86×10^{-6}	1.84	4.96×10^{-6}
4.41	528.3083	ND	ND	0.26	2.01×10^{-6}	3.26	2.50×10^{-6}
3.62	512.2981	$[M+FA]^-$	LysoPC(14:0)	0.50	3.01×10^{-6}	1.90	3.71×10^{-6}
5.81	255.2321	[M-H]	(16/0) Palmitic acid	0.44	3.62×10^{-6}	1.75	1.21×10^{-5}
4.10	540.3247	$[M+FA]^-$	LysoPC(16:0)	0.77	3.75×10^{-6}	1.32	1.98×10^{-5}
5.20	277.2150	$[M-H]^-$	(18/3n-6) Gamma-Linolenic acid	0.41	4.15×10^{-6}	1.85	7.34×10^{-5}
4.37	297.2425	ND	ND	0.39	4.35×10^{-6}	1.91	7.04×10^{-4}
5.80	305.2474	$[M-H]^-$	(20/3n-9) 5,8,11-Eicosatrienoic acid	0.28	6.07×10^{-6}	2.07	5.61×10^{-3}
5.20	301.2155	$[M-H]^-$	(20/5n-3) 5,8,11,14,17-Eicosapentaenoic acid	0.32	7.38×10^{-6}	2.23	2.33×10^{-4}
4.00	500.2761	$[M-H]^-$	LysoPE(20:4)	0.51	1.08×10^{-5}	1.79	1.42×10^{-4}
3.02	423.1231	ND	ND	0.21	1.42×10^{-5}	4.53	4.72×10^{-5}
2.59	300.2017	ND	ND	0.47	1.50×10^{-5}	2.11	2.30×10^{-4}
3.68	586.3120	$[M+FA]^-$	LysoPC(20:5)	0.30	1.77×10^{-5}	2.28	1.98×10^{-4}
5.37	321.2028	ND	ND	0.25	1.81×10^{-5}	2.65	7.38×10^{-4}
3.94	552.3198	$[M+FA-MFA]^-$	LysoPC(22:6)	0.53	1.86×10^{-5}	1.80	1.34×10^{-5}
5.03	277.2156	$[M-H]^-$	(18/3n-3) Alpha-Linolenic acid	0.32	3.78×10^{-5}	2.27	6.49×10^{-5}
7.57	944.5649	ND	ND	1.61	3.82×10^{-5}	0.57	1.79×10^{-4}
2.66	326.7101	ND	ND	0.41	4.14×10^{-5}	2.70	1.51×10^{-4}
3.93	588.3280	$[M+FA]^-$	LysoPC(20:4)	0.53	4.26×10^{-5}	1.96	3.45×10^{-6}
5.99	603.2928	ND	ND	0.35	4.38×10^{-5}	1.57	2.31×10^{-5}
4.30	566.3456	$[M+FA]^-$	LysoPC(18:1)	0.61	4.68×10^{-5}	2.95	3.04×10^{-5}
2.58	195.1178	ND	ND	0.36	5.15×10^{-5}	2.35	1.51×10^{-4}
2.66	652.4113	ND	ND	0.47	5.71×10^{-5}	2.02	8.87×10^{-6}
4.00	524.2758	$[M-H]^-$	LysoPE(22:6)	0.53	5.76×10^{-5}	1.98	1.11×10^{-4}
2.60	388.2538	ND	ND	0.53	5.95×10^{-5}	2.46	7.18×10^{-5}
5.67	329.2474	$[M-H]^-$	(22/5n-3) 7,10,13,16,19-Docosapentaenoic acid	0.33	6.06×10^{-5}	1.50	3.44×10^{-3}
5.99	281.2479	$[M-H]^-$	(18/1n-9) Oleic acid	0.49	6.09×10^{-5}	1.82	2.49×10^{-6}
4.02	612.3282	$[M+FA]^-$	LysoPC(22:6)	0.58	6.12×10^{-5}	1.31	4.63×10^{-4}
3.97	564.3266	$[M+FA]^-$	LysoPC(18:2)	0.71	9.93×10^{-5}	1.74	5.97×10^{-5}
6.01	331.2632	$[M-H]^-$	(22/4n-6) 7,10,13,16-Docosatetraenoic acid	0.47	1.03×10^{-4}	1.68	8.65×10^{-6}
4.02	588.3294	$[M+FA]^-$	LysoPC(20:4)	0.60	1.08×10^{-4}	1.35	4.59×10^{-2}
3.93	476.2758	$[M-H]^-$	LysoPE(18:2)	0.59	1.22×10^{-4}	2.03	2.96×10^{-4}
6.11	281.2470	$[M-H]^-$	(18/1n-x)	0.40	2.88×10^{-4}	2.33	9.40×10^{-5}
5.99	621.3031	ND	ND	0.36	3.01×10^{-4}	1.83	3.35×10^{-5}
6.66	638.4756	$[M+FA]^-$	PC(O-24:0/0:0)	0.52	4.04×10^{-4}	2.31	9.07×10^{-5}
6.80	733.5489	$[M+FA]^-$	SM(d18:1/15:0)	0.57	4.23×10^{-4}	2.02	1.01×10^{-7}
5.83	329.2474	$[M-H]^-$	(22/5n-6) 4,7,10,13,16-Docosapentaenoic acid	0.42	4.35×10^{-5}	1.92	5.42×10^{-5}
5.49	327.2314	$[M-H]^-$	(22/6n-3) 4,7,10,13,16,19-Docosahexaenoic acid	0.48	6.43×10^{-4}	1.88	6.99×10^{-6}
4.39	494.3241	$[M+FA-MFA]^-$	LysoPC(17:0)	0.62	7.43×10^{-4}	2.63	1.30×10^{-6}
5.55	303.2318	$[M-H]^-$	(20/4n-6) Arachidonic acid	0.50	1.04×10^{-3}	1.52	1.34×10^{-4}

Peaks are listed for which there is significant correlation of wild-type samples with age [test *P*-values < 0.05]. *Rt* (min), chromatographic retention time; *m/z* (Da/e) [*m* is the neutral molecular mass value, *e* is the elemental charge], mass-to-charge ratio of ion detected; Ion, most intense species observed; ID, metabolite name (lipid names follow the LIPID MAPS classification system for lipids www.lipidmaps.org); ND, not determined.

age-associated metabolic decline (Figures 3 and 4). These results suggest metabolic changes related to the aging process that can be reverted after treatment with AAV9-mTERT. Interestingly, some of the metabolites identified in the gene therapy with AAV9-mTERT, were similar to those identified in the metabolic signature of aging. When we specifically studied some of these metabolites in the different exper-

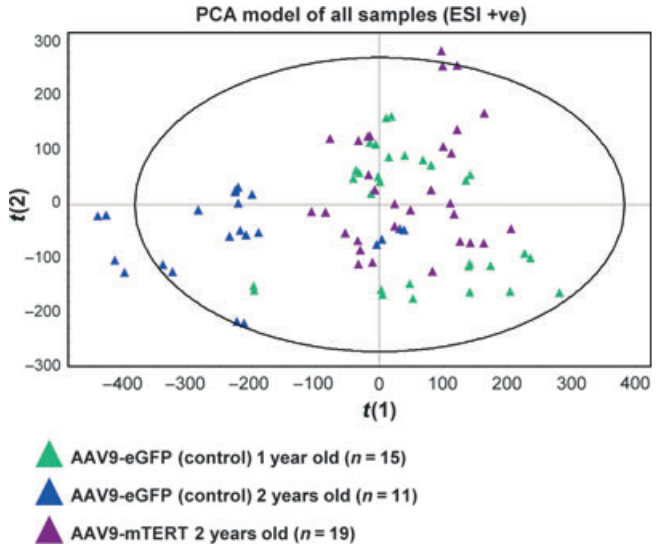

Fig. 3 PCA score plot discriminating 2-year-old AAV9-GFP from 2-year-old AAV9-GFP and 2-year-old AAV9-mTERT-treated mice. Duplicate sample injection data are shown (duplicate sample extracts were injected in each ionization mode as quality controls).

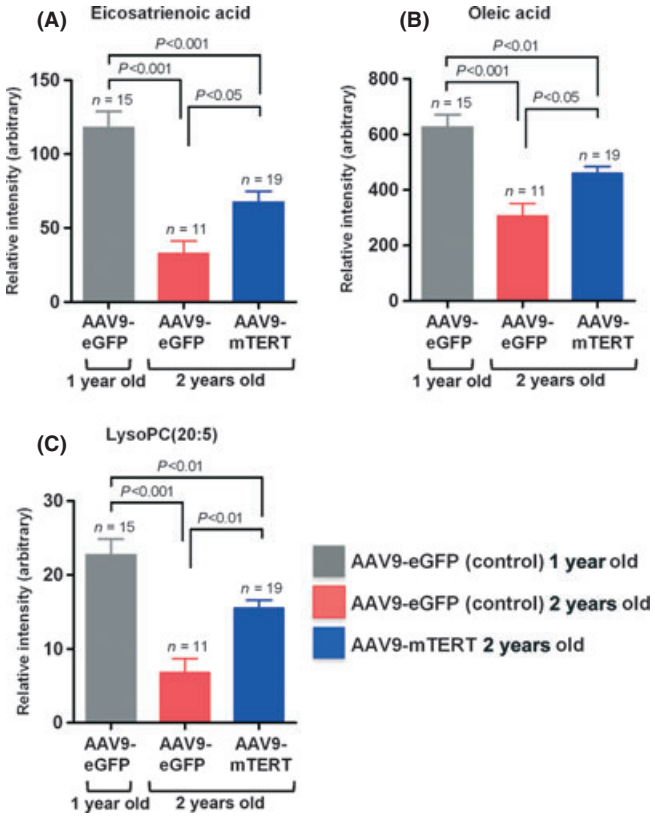

Fig. 4 Profile plot of biomarkers. Raw intensity data, including average group intensities, number of samples and *P*-values, corresponding to the highlighted biomarkers: (A) Eicosatrienoic acid; (B) Oleic acid; (C) LysoPC (20:5).

imental groups (Fig. 4), we confirmed that their decrease associated with aging and that this decline was significantly reversed by TERT treatment.

The existence of a metabolomic signature suggests that aging is accompanied by predictable metabolomic changes. This is akin to other aging-associated features that reflect on the appearance of tissues or on the performance of physiological systems. It is conceivable that physiological decline in important metabolic organs, such as liver, muscle, pancreas, or adipose tissue, will reflect on the serum metabolite pattern. The identification of this signature is a first step to understand the metabolic alterations associated with aging and guides anti-aging interventions targeting metabolism. Recently, a study in humans demonstrated that metabolic profiles are age dependent and might reflect different aging processes, such as incomplete mitochondrial fatty acid oxidation (Yu *et al.*, 2012), demonstrating the importance of age-related metabolomic profiles.

The age biomarkers identified here include lipids and other small molecules such as creatine, methionine, and uric acid. Whether these biomarkers play a role in aging or are due to secondary phenomena will require further investigation. Aberrant lipid homeostasis has been linked to a number of age-related diseases, including cardiovascular disease, inflammation, metabolic syndrome, and type II diabetes (Maxfield & Tabas, 2005). Creatine deficiency is associated with muscle loss (sarcopenia), a common condition in the elderly (Pearlman & Fielding, 2006; Brosnan & Brosnan, 2007). Moreover, creatine synthesis makes major demands of methionine (Brosnan & Brosnan, 2007), another biomarker identified in this study whose levels decrease with age. Uric acid, which was found to increase with age, correlates with several risk factors, including renal dysfunction, hypertension, insulin resistance, and cardiovascular disease (Feig *et al.*, 2008). A recent study using three different long-lived mouse models (caloric restriction, insulin receptor substrate 1 knockout, and Ames dwarf) has identified several plasma biomarkers of aging using 1H NMR spectroscopy (Wijeyesekera *et al.*, 2012). In this study, a panel of metabolic differences was generated for each model relative to their controls, and then, the three models were compared with one another. Although the age biomarkers identified by this approach differed between the three models, they also included lipids, such as phosphatidylcholine, and small molecules (methionine, choline, and creatinine) that are coincident with our present findings. Taken together, these results suggest that changes in lipid homeostasis and one-carbon metabolism may be associated with the aging process.

Finally, the fact that metabolomic changes associated with natural mouse aging can also predict aging provoked by accelerated telomere shortening owing to telomerase deficiency provides strong evidence that telomere loss significantly contributes to natural mouse aging. This is further substantiated by our findings that TERT treatment is able to reverse some of the metabolic changes associated with aging. In a similar manner, the metabolomic signature described here can be used to enquire the contribution of other molecular pathways (i.e., tumor suppression) to natural mouse aging, as well as to estimate the impact of genetic modifications or treatments on mouse aging.

Materials and methods

Mice and samples

Mice were generated and housed at the Spanish National Cancer Research Center barrier area, where pathogen-free procedures are employed in all mouse rooms [specific pathogen-free (SPF), and health status is assured through a comprehensive health surveillance program]. Mice were under controlled room temperature and fed *ad libitum* with an irradiated diet (n° 2018, Harlan). All genetic backgrounds were kept

under the same conditions. Wild-type mice used to establish a metabolomic signature of aging were from the following mouse lines maintained at the CNIO: AZD (*SuperSIRT*$^{+/+}$; 100% C57BL/6 background) (*Pfluger et al.*, 2008), AIU (*ATM*$^{+/+}$; mixed C57BL/6-129sv background) (Barlow *et al.*, 1996), RFC (*Terc*$^{+/+}$; 100% C57BL/6 background) (Blasco *et al.*, 1997), RSZ (wild-type controls for *Sp53/Sp16/SARF/TgTert* and *Sp53/Sp16/SARF* transgenics both of a mixed 75% C57BL/6-25% DBA/2 background) (Tomas-Loba *et al.*, 2008), RPR (wild-type controls for *K5-TRF2/K5-TERT*; mixed 75% C57BL/6-25% DBA/2 background) (Munoz *et al.*, 2005), RPP (wild-type controls for *K5-TRF2/G1Terc*$^{-/-}$; 100% C57BL/6 background) (Munoz *et al.*, 2005), RPT (*XPF*$^{+/+}$; mixed C57BL/6-129sv background) (Tian *et al.*, 2004), and RXS (wild-type controls for *K5-TERT* both mixed 75% C57BL/6-25% DBA/2 and 100% C57BL/6 backgrounds) (Gonzalez-Suarez *et al.*, 2001). Mutant mouse lines used for comparative purposes were *Sp53/Sp16/SARF* and *Sp53/Sp16/SARF/TgTert* (mixed 75% C57BL/6-25% DBA/2 background), *K5-TERT* (mixed 75% C57BL/6-25% DBA/2 background), and G1 *Terc*$^{-/-}$ (pure C57BL/6 background) (Gonzalez-Suarez *et al.*, 2001; Matheu *et al.*, 2007; Tomas-Loba *et al.*, 2008).

Mice studied for TERT-based gene therapy have been previously described (Bernardes de Jesus *et al.*, 2012). Separate groups of mice were tail-vein-injected with 2×10^{12} vg (viral genomes)/animal of either AAV9-GFP at 1 year old (AAV9-GFP, $n = 15$ [47% males]) or AAV9-GFP and AAV9-mTERT at 2 years old (AAV9-GFP, $n = 11$ [36% males]; AAV9-mTERT, $n = 19$ [58% males]. Sera were collected between 1 to 2 months post-telomerase treatment.

Samples were extracted from facial vein before 12 AM after overnight fasting and collected in tubes without any anticoagulant. The samples were collected in a SPF area of CNIO and kept at room temperature until leaving this area (15–20 min). Samples were maintained in ice for 10 additional minutes and centrifuged at 4°C. The serum supernatant was then aliquoted and frozen at −80°C, to minimize freeze–thaw degradation, until they were analyzed. For all the samples, the procedure was the same. Procedures for sample extraction and storage were similar to those employed in other wide-coverage metabolomics approaches (Dunn *et al.*, 2011).

Housed mice followed the recommendations of the Federation of European Laboratory Animal Science Associations.

Metabolic profiling

A global metabolite profiling UPLC®-MS methodology was employed where all endogenous metabolite-related features, characterized by their mass-to-charge ratio *m/z* and retention time *Rt*, are included in a subsequent multivariate analysis procedure used to study metabolic correlation between spectral data and age in the WT samples. Using the model built, age predictions of transgenic samples were obtained. Where possible, *Rt-m/z* features corresponding to putative biomarkers were later identified. Sample preparation and LC/MS analysis were performed as described in detail previously (Barr *et al.*, 2010). Briefly, liquid–liquid extraction of the metabolites was performed by protein precipitation of 50 μL defrosted serum with four volumes of methanol. After brief vortex mixing, the samples were incubated overnight at −20°C. Supernatants were collected after centrifugation at 13 000 rpm for 10 min and transferred to vials for UPLC®-MS analysis. Chromatography was performed on a 1-mm i.d. × 100 mm ACQUITY 1.7 μm C8 BEH column (Waters Corp., Milford, CT, USA) using an ACQUITY UPLC® system (Waters Corp.). The volume of sample injected onto the column was 2 μL. The eluent was introduced into the mass spectrometer (QTOF Premier, Waters Corp.) by electrospray ionization, with capillary and cone voltages set in the positive and negative ion modes to 3200, 30, 2800, and 50 V, respectively. The nebulization gas was set to 600 L h^{-1} at a temperature of 350°C. The cone gas was set to 30 L h^{-1}, and the source temperature was set to 150°C. All spectra were mass corrected in real time by reference to leucine enkephalin, infused at 50 μL/min through an independent reference electrospray, sampled every 10 s. An appropriate test mixture of standard compounds was analyzed before and after the entire set of randomized, duplicated sample injections to examine the retention time stability (generally < 6 s variation, injection-to-injection), mass accuracy (generally < 3 ppm for *m/z* 400–1000, and < 1.2 mDa for *m/z* 50–400), and sensitivity of the system throughout the course of the run, which lasted a maximum of 26 h per batch of samples injected.

The analytical methodology was designed to provide maximum coverage over phospholipids, fatty acids, and organic acids, while offering relatively high-throughput with minimum injection-to-injection carryover effects.

Data analysis

All data were processed using the MarkerLynx application manager for MassLynx 4.1 software (Waters Corp.). The LC/MS data are peak-detected and noise-reduced in both the LC and MS domains such that only true analytical peaks are further processed by the software (e.g., noise spikes are rejected). A list of intensities (chromatographic peak areas) of the peaks detected is then generated for the first chromatogram, using the *Rt-m/z* data pairs as identifiers. This process is repeated for each LC-MS analysis and the data sorted such that the correct peak intensity data for each *Rt-m/z* pair are aligned in the final data table. The ion intensities for each peak detected are then normalized, within each sample, to the sum of the peak intensities in that sample. There were no significant differences ($F < F_{crit}$) between the total intensities used for normalization and the sample groups being compared in the study. The resulting normalized peak intensities form a single matrix with *Rt-m/z* pairs for each file in the data set. All processed data, positive and negative ion modes, were mean centered and unit variance scaled during multivariate data analysis.

Multivariate data analysis

The first objective in the data analysis process was to create a multivariate model able to correlate the spectral data and WT samples' age. The predictive multivariate modeling was carried out using the SIMCA – P+ (version 12.0.1; Umetrics, Sweden) software. Projection to latent structure (PLS) is a very useful statistical technique when there are more highly correlated prediction variables (multicollinearity). This supervised pattern recognition method relates the two data matrices, *for example, Rt-m/z* pair data (*X* matrix) and age (*Y* matrix), extracting the limited number of latent factors (which are linear combinations of the original prediction variables) that explain as much as possible the covariance matrices and allowing that the response variable *Y* could be predicted from *X*. The performance of the PLS model was evaluated using the R^2Y and Q^2 parameters. R^2Y provides an indication of how much of the variation within the data set can be explained by the model. Q^2 parameter describes the predictive ability of model to estimate the *Y* data (a Q^2 score between 0.6–1.0 is indicative of a reliable classifier).

Validation of PLS models

The best validation of a model is the analysis of an independent and representative set of samples that does not form part of the model-building population. However, the reduced sample size of wild-type mice

over 100 weeks old, necessary for the prediction of the long-lived TERT transgenic mice, limited the splitting of the samples into a test and a validation group. As recommended by Wold *et al.*, 2001, we followed two ways of PLS model validation: cross-validation and model re-estimation. Component-wise cross-validation was carried out, calculating R^2Y and Q^2 parameters by iteratively leaving out one-seventh of the samples from the model and predicting their group classification. Paired-sample injections were randomly distributed over the cross-validation groups (7-fold), minimizing the risk of calculating falsely predictive components. Additionally, 200 parallel PLS models permuting randomly the *Y* data with respect to their related *X* data set were generated. The comparison of the estimated values of R^2Y and Q^2 of the parallels and original model gives an indication of the statistical significance of the predictive power of the PLS model. If the original model is valid, randomization of the *Y* data would be expected to considerably reduce Q^2. As can be seen in Supplementary Figure 1, most of the models obtained through this randomization were nonpredictive (negative Q^2).

Predictions of transgenic samples

PLS model from WT samples was used to predict ages of mice lacking telomerase activity (G1 *Terc*$^{-/-}$), overexpressing telomerase reverse transcriptase (K5-Tert), simultaneously overexpressing K5-Tert, p53, and p19ARF, and overexpressing p53 and p19ARF.

Differences between transgenic and WT-predicted ages were evaluated by calculating the unpaired student's *t*-test *P*-values after data normalization with respect the real age.

Metabolite biomarker selection according to the age correlation

Variable influence on projection in PLS model statistic represents the value of each *X* variable in fitting the PLS model, measuring the importance of those variables with respect to its correlation to the *Y* data. In the present work, *Rt-m/z* pair data with a larger VIP value are the most influential for the model, and those with VIP values lower than 0.7 are considered to have small contribution to the prediction.

Additionally, Spearman's rank correlation coefficient (ρ) for each selected metabolite biomarker was calculated. The Spearman correlation coefficient is a nonparametric measure of correlation between two variables, indicating with the sign the direction of association between the independent variable (*Rt-m/z* pair) and the dependent variable (Age), *for example,* if age variable tends to increase when *Rt-m/z* pair increases, the Spearman correlation coefficient is positive. Only *P*-values derived from the Spearman's rank correlation coefficient lower than 0.05 were considered in the metabolite biomarker selection.

Multivariate analysis of AAV9-eGFP and AAV9-mTERT mice

Principal components analysis (PCA) of the data set was performed to enable easy visualization of any metabolic clustering of the different groups of samples (Fig. 3). In PCA, the data matrix is reduced to a series of principal components (PCs), each with a linear combination of the original *Rt-m/z* pair peak areas. Each successive PC explains the maximum amount of variance possible, not accounted for by the previous PCs.

The orthogonal partial least squares to latent structures discriminant analysis (OPLS-DA) method were used for the identification of metabolites contributing to the clustering observed in the PCA plots. The performance of the OPLS-DA model was evaluated using Q^2Y parameter, which describes the predictive ability of model to estimate the *Y* data, and calculated by iteratively leaving out samples from the model and predicting their group classification. Paired-sample injections were randomly distributed over the cross-validation groups (7-fold), minimizing the risk of calculating falsely predictive components. Appropriate filtration of the loading profile associated with the OPLS-DA predictive components resulted in a set of candidate biomarkers that were further evaluated by calculating group percentage changes and unpaired Student's *t*-test *P*-values.

One-way ANOVA with Tukey's multiple comparison test has been used for statistical comparisons of Fig. 4.

Metabolite biomarker identification

Exact molecular mass data from redundant *m/z* peaks corresponding to the formation of different parent (e.g., cations in the positive ion mode, anions in the negative ion mode, adducts, multiple charges) and product (formed by spontaneous 'in-source' CID) ions were first used to help confirm the metabolite molecular mass. This information was then submitted for database searching, either in-house or using the online ChemSpider database (www.chemspider.com) where the Kegg, Human Metabolome Database, and Lipid Maps data source options were selected. MS/MS data analysis highlights neutral losses or product ions, which are characteristic of metabolite groups and can serve to discriminate between database hits.

Acknowledgments

We are indebted to Cristina Alonso and Jonathan Barr from OWL for generation and analysis of the metabolomic profiles. Work in the laboratory of M.A.B. was funded by Spanish Ministry of Science and Innovation Projects SAF2008-05384 and CSD2007-00017, European Union FP7 Projects 2007-A-201630 (GENICA) and 2007-A-200950 (TELOMARKER), European Research Council Advanced Grant GA#232854, Körber Foundation, Fundación Botín, and Fundación Lilly. Work in the laboratory of J.M.M is funded by grants from the MICINN (CIBERehd), the European Union (HEPADIP), the NIH (AT-1576, AT-4896), and ETORTEK-2008.

Author contributions

A.T-L. generated the mice presented in Figs. 1 and 2 of the study and collected the samples. B.B.J. generated the mice presented in Figs. 3 and 4 of the study and collected the samples. M.A.B. and J.M.M. designed the experimental plan, analyzed and interpreted the data. M.A.B. directed the project and wrote the paper.

Disclosures

M.A.B. is a co-founder of Life Length; S.L. a biotechnology company that commercializes telomere length tests; and J.M.M. is a co-founder of OWL, a metabolomics-based biotechnology company.

References

Allen J, Davey HM, Broadhurst D, Heald JK, Rowland JJ, Oliver SG, Kell DB (2003) High-throughput classification of yeast mutants for functional genomics using metabolic footprinting. *Nat. Biotechnol.* **21**, 692–696.

Barlow C, Hirotsune S, Paylor R, Liyanage M, Eckhaus M, Collins F, Shiloh Y, Crawley JN, Ried T, Tagle D, Wynshaw-Boris A (1996) Atm-deficient mice: a paradigm of ataxia telangiectasia. *Cell* **86**, 159–171.

Barr J, Vazquez-Chantada M, Alonso C, Perez-Cormenzana M, Mayo R, Galan A, Caballeria J, Martin-Duce A, Tran A, Wagner C, Luka Z, Lu SC, Castro A, Le Marchand-Brustel Y, Martinez-Chantar ML, Veyrie N, Clement K, Tordjman J, Gual P, Mato JM (2010) Liquid chromatography-mass spectrometry-based

parallel metabolic profiling of human and mouse model serum reveals putative biomarkers associated with the progression of nonalcoholic fatty liver disease. *J. Proteome Res.* **9**, 4501–4512.

Bernardes de Jesus B, Vera E, Schneeberger K, Tejera AM, Ayuso E, Bosch F, Blasco MA (2012) Telomerase gene therapy in adult and old mice delays aging and increases longevity without increasing cancer. *EMBO Mol. Med.* **4**, 1–14.

Blasco MA, Lee HW, Hande MP, Samper E, Lansdorp PM, DePinho RA, Greider CW (1997) Telomere shortening and tumor formation by mouse cells lacking telomerase RNA. *Cell* **91**, 25–34.

Brosnan JT, Brosnan ME (2007) Creatine: endogenous metabolite, dietary, and therapeutic supplement. *Annu. Rev. Nutr.* **27**, 241–261.

Cutler RG, Mattson MP (2001) Sphingomyelin and ceramide as regulators of development and lifespan. *Mech. Ageing Dev.* **122**, 895–908.

Dunn WB, Broadhurst D, Begley P, Zelena E, Francis-McIntyre S, Anderson N, Brown M, Knowles JD, Halsall A, Haselden JN, Nicholls AW, Wilson ID, Kell DB, Goodacre R (2011) Procedures for large-scale metabolic profiling of serum and plasma using gas chromatography and liquid chromatography coupled to mass spectrometry. *Nat. Protoc.* **6**, 1060–1083.

Feig DI, Kang DH, Johnson RJ (2008) Uric acid and cardiovascular risk. *N. Engl. J. Med.* **359**, 1811–1821.

Garcia-Cao I, Garcia-Cao M, Tomas-Loba A, Martin-Caballero J, Flores JM, Klatt P, Blasco MA, Serrano M (2006) Increased p53 activity does not accelerate telomere-driven ageing. *EMBO Rep.* **7**, 546–552.

Gonzalez-Suarez E, Samper E, Ramirez A, Flores JM, Martin-Caballero J, Jorcano JL, Blasco MA (2001) Increased epidermal tumors and increased skin wound healing in transgenic mice overexpressing the catalytic subunit of telomerase, mTERT, in basal keratinocytes. *EMBO J.* **20**, 2619–2630.

Gonzalez-Suarez E, Geserick C, Flores JM, Blasco MA (2005) Antagonistic effects of telomerase on cancer and aging in K5-mTert transgenic mice. *Oncogene* **24**, 2256–2270.

Herrera E, Samper E, Martin-Caballero J, Flores JM, Lee HW, Blasco MA (1999) Disease states associated with telomerase deficiency appear earlier in mice with short telomeres. *EMBO J.* **18**, 2950–2960.

Klunk WE, Xu CJ, McClure RJ, Panchalingam K, Stanley JA, Pettegrew JW (1997) Aggregation of beta-amyloid peptide is promoted by membrane phospholipid metabolites elevated in Alzheimer's disease brain. *J. Neurochem.* **69**, 266–272.

Lee HW, Blasco MA, Gottlieb GJ, Horner JW, 2nd , Greider CW, DePinho RA (1998) Essential role of mouse telomerase in highly proliferative organs. *Nature* **392**, 569–574.

Lewis GD, Farrell L, Wood MJ, Martinovic M, Arany Z, Rowe GC, Souza A, Cheng S, McCabe EL, Yang E, Shi X, Deo R, Roth FP, Asnani A, Rhee EP, Systrom DM, Semigran MJ, Vasan RS, Carr SA, Wang TJ, Sabatine MS, Clish CB, Gerszten RE (2010) Metabolic signatures of exercise in human plasma. *Sci. Transl. Med.* **2**, 33ra37.

Matheu A, Maraver A, Klatt P, Flores I, Garcia-Cao I, Borras C, Flores JM, Vina J, Blasco MA, Serrano M (2007) Delayed ageing through damage protection by the Arf/p53 pathway. *Nature* **448**, 375–379.

Maxfield FR, Tabas I (2005) Role of cholesterol and lipid organization in disease. *Nature* **438**, 612–621.

Munoz P, Blanco R, Flores JM, Blasco MA (2005) XPF nuclease-dependent telomere loss and increased DNA damage in mice overexpressing TRF2 result in premature aging and cancer. *Nat. Genet.* **37**, 1063–1071.

Nicholson JK, Wilson ID (2003) Opinion: understanding 'global' systems biology: metabonomics and the continuum of metabolism. *Nat. Rev. Drug. Discov.* **2**, 668–676.

Pearlman JP, Fielding RA (2006) Creatine monohydrate as a therapeutic aid in muscular dystrophy. *Nutr. Rev.* **64**, 80–88.

Pfluger PT, Herranz D, Velasco-Miguel S, Serrano M, Tschop MH (2008) Sirt1 protects against high-fat diet-induced metabolic damage. *Proc. Natl Acad. Sci. USA* **105**, 9793–9798.

Raamsdonk LM, Teusink B, Broadhurst D, Zhang N, Hayes A, Walsh MC, Berden JA, Brindle KM, Kell DB, Rowland JJ, Westerhoff HV, van Dam K, Oliver SG (2001) A functional genomics strategy that uses metabolome data to reveal the phenotype of silent mutations. *Nat. Biotechnol.* **19**, 45–50.

Tian M, Shinkura R, Shinkura N, Alt FW (2004) Growth retardation, early death, and DNA repair defects in mice deficient for the nucleotide excision repair enzyme XPF. *Mol. Cell. Biol.* **24**, 1200–1205.

Tomas-Loba A, Flores I, Fernandez-Marcos PJ, Cayuela ML, Maraver A, Tejera A, Borras C, Matheu A, Klatt P, Flores JM, Vina J, Serrano M, Blasco MA (2008) Telomerase reverse transcriptase delays aging in cancer-resistant mice. *Cell* **135**, 609–622.

Vera E, Bernardes de Jesus B, Foronda M, Flores JM, Blasco MA (2012) The rate of increase of short telomeres predicts longevity in mammals. *Cell Rep.* **2**, 732–737.

Wijeyesekera A, Selman C, Barton RH, Holmes E, Nicholson JK, Withers DJ (2012) Metabotyping of long-lived mice using 1H NMR spectroscopy. *J. Proteome Res.* **11**, 2224–2235.

Wold S, Sjöström M, Eriksson L (2001) PLS-regression: a basic tool of chemometrics. *Chemometr. Intell. Lab. Syst.* **58**, 109–130.

Yu Z, Zhai G, Singmann P, He Y, Xu T, Prehn C, Romisch-Margl W, Lattka E, Gieger C, Soranzo N, Heinrich J, Standl M, Thiering E, Mittelstrass K, Wichmann HE, Peters A, Suhre K, Li Y, Adamski J, Spector TD, Illig T, Wang-Sattler R (2012) Human serum metabolic profiles are age dependent. *Aging Cell* **11**, 960–967.

Supporting Information

Additional Supporting Information may be found in the online version of this article at the publisher's web-site.

Figure S1. Validation of WT aging – PLS model by permuting randomly the Age data with respect to the *X* data set. These re-estimations of the model evaluate the probability to obtain a good fit with random response data. R^2 parameter (green triangles) estimates how well the model fits the data, and Q^2 parameter (blue squares) provides an estimate of how well the model predicts the age data. Permutation of age data reduces considerably Q^2, being negative or nonpredictive for most of the re-estimated models.